CORRELATING REFLECTANCE AND X-RAY SPECTROSCOPIC DATA FROM MESSENGER. Noam R. Izenberg (noam.izenberg@jhuapl.edu)[1], Shoshana Z. Weider[2], Larry R. Nittler[2], and Sean C. Solomon[2,3]. [1]The Johns Hopkins University Applied Physics Laboratory, Laurel, MD 20723, USA. [2]Department of Terrestrial Magnetism, Carnegie Institution of Washington, Washington, DC 20015, USA. [3]Lamont-Doherty Earth Observatory, Columbia University, Palisades, NY 10964, USA.

Introduction: The MErcury Surface, Space ENvironment, GEochemistry, and Ranging (MESSENGER) spacecraft's [1] Mercury Atmospheric and Surface Composition Spectrometer (MASCS) [2] and X-Ray Spectrometer (XRS) instruments have been mapping the planet's surface and exosphere from orbit since 29 March 2011. MASCS has obtained more than 3 million surface reflectance spectra at near-ultraviolet to near-infrared wavelengths to date. The MASCS Visible and Infrared Spectrograph (VIRS) operates over the wavelength range 300–1450 nm. VIRS reflectance spectra show no clear evidence of an absorption band centered at a wavelength near ~1 μm (1000 nm) that would be diagnostic of the presence of ferrous iron in silicates. However, ultraviolet (UV) absorptions do show some spectral slope variation at wavelengths shorter than ~400 nm. The UV variations are consistent with the low total Fe abundances (averaging ~1–2 wt%) on Mercury's surface indicated by fluorescent X-ray spectra obtained by XRS [3-5] as well as MESSENGER's Gamma-Ray Spectrometer (GRS) [6] and even lower abundances for ferrous iron in silicates [7]. XRS results show that Mercury's crust is Mg-rich but Al- and Ca-poor relative to typical terrestrial and lunar rocks and has a high abundance of S [3-5]. The absolute abundances are subject to systematic uncertainties, amounting to perhaps a factor of 2 for Fe, but relative differences across the planet's surface are more robust [5].

VIRS Mapping: Systematic VIRS mapping of Mercury has sampled over 90% of the planet on a spatial scale of 20 km. Figure 1 is a red-green-blue (RGB) composite of VIRS reflectance values (with an emprical photometric correction) and ratios overlaid on a Mercury Dual Imaging System (MDIS) [8] base map. The red channel is MASCS VIRS reflectance at 575 nm (R575), which is a proxy for visible albedo; the green channel is the 415 nm/750 nm reflectance ratio (VISr), which is a proxy for the visible-near infrared spectral slope; and the blue channel is the 310 nm/390 nm reflectance ratio (UVr), which indicates the relative strength of UV absorption features. This composite highlights locations on Mercury's surface that are distinct from the planetary average spectral signature [9, 10]. These regions can be categorized to give a set of spectral units that correlate with MDIS color units and geomorphology [9, 10]. Mercury's "average" spectral unit consists mostly of plains units, with R575, VISr, and UVr values close to the means for Mercury. The volcanic northern plains and Caloris interior plains (labeled a and b, respectively, in Fig. 1) tend to have high R575 and low UVr values (purple-red-yellow color in Fig. 1), whereas areas such as the circum-Caloris plains (labeled c in Fig. 1), Rembrandt basin (labeled 10 in Fig. 1), and the area around Nabokov crater (labeled 1 and 2 in Fig. 1) have high UVr values (cyan-purple color in Fig. 1).

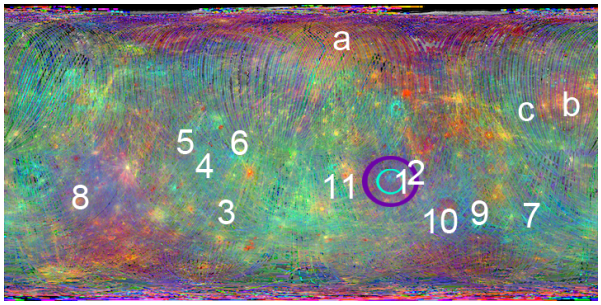

Figure 1. Composite MASCS VIRS global coverage map overlaid on MDIS monochrome mosaic. Individual MASCS footprints are represented in colors indicating spectral properties (refer to text for color assignments). Numbers and letters mark regions of interest noted in the text.

XRS Mapping: The most complete compositional information derived from XRS data is limited to regions of the planet that were observed during periods of solar flares [3–5]. Because of MESSENGER's eccentric orbit, the spatial resolution of XRS footprints increases toward high northern latitudes. Areas mapped so far by XRS during solar flare periods [3-5] are shown in Figure 2. The large footprints that span the southern hemisphere relate to the strongest solar flares, from which abundance data for Mg, Al, S, Ca, and Fe can be derived [3-5]. The smaller footprints in the northern hemisphere are from weaker flares when only Mg, Al, S, and Ca abundances can be estimated [3, 4]. In the XRS RGB composite (Fig. 2), the red channel is S/Si, the green channel is Ca/Si, and the blue channel is Fe/Si. This color scheme highlights areas with the highest Fe (blue), S (yellow-orange), and Ca (green). The high-Fe region (labeled 1, 2 in Fig. 1) has an Fe/Si ratio of 0.07, equivalent to ~1.5 wt % Fe. The dark green area (labeled 3 in Fig. 1) has the lowest Fe/Si ratio of 0.01 (~0.2 wt % Fe).

MASCS–XRS Comparison: Because of the incomplete global coverage of XRS observations, direct comparison between MASCS and XRS data must be confined to areas that have been observed by both instruments. We focus here on the areas observed by XRS for which there is Fe abundance information from at least two overlapping XRS footprints (i.e., the southern hemisphere) [5]. The regions we compare were chosen to

provide a representative sampling of the range in XRS-derived compositions. The regions are numbered in all figures as follows: (1) Nabokov crater; (2) Nabokov and surrounding region; (3) plains with low Fe/Si; (4) plains with low Fe/Si, high S/Si, and high Ca/Si; (5) plains with low Fe/Si and high S/Si; (6) plains with high S/Si; (7) plains with high Ca/Si; (8) and (9) regions with average XRS elemental ratio values; (10) Rembrandt basin; and (11) Ellington crater region.

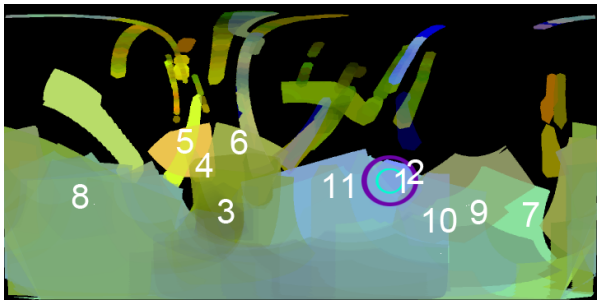

Figure 2. RGB color composite for XRS-derived surface composition [4, 5]. Red: S abundance; green: Ca abundance; blue: Fe abundance. Number labeling is as in Figure 1.

Discussion: For each of the 11 regions we compared the MASCS R575, VISr, and UVr parameters to the XRS-derived S/Si, Ca/Si, and Fe/Si values. The best correlation is between UVr and Fe/Si (Fig. 3). The UVr parameter is likely being influenced by Fe oxygen–metal charge transfer absorptions that occur in the near-UV [9, 10], and it is therefore at least partially representative of Fe content. If the correlation is verified by additional data, then it may be possible to extrapolate that regions with higher UVr values (>0.7), e.g., areas that contain hollows [11, 12] or low-reflectance plains [13], have higher than average Fe contents (>4 wt % Fe).

The only other parameter comparison that may indicate a relationship is between the MASCS UVr and XRS S/Si (Fig. 4). Although low-sulfur regions have no apparent relation to UVr, the region with the highest S/Si ratio (labeled as 5 in all figures) has a low UVr value. This region is adjacent to that with the lowest Fe and itself has a below-average UVr value. This outcome is in contrast to an XRS S/Si–Fe/Si correlation observed elsewhere on the planet [5] and suggests that the highest S contents may be found in the low-Fe regions.

We note that the center of Nabokov crater has a much higher UVr value than the extended Nabokov region, which is within the high Fe/Si area. It is possible that the poor XRS spatial resolution in the southern hemisphere smears out a higher concentration of Fe in Nabokov crater to give the appearance of a more spatially extended high-Fe region.

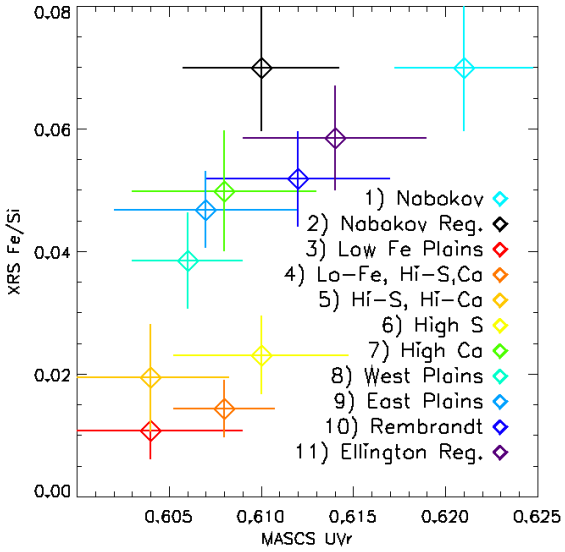

Figure 3. MASCS UVr versus XRS Fe/Si for the series of locations marked in Figs. 1 and 2. Approximate errors are shown.

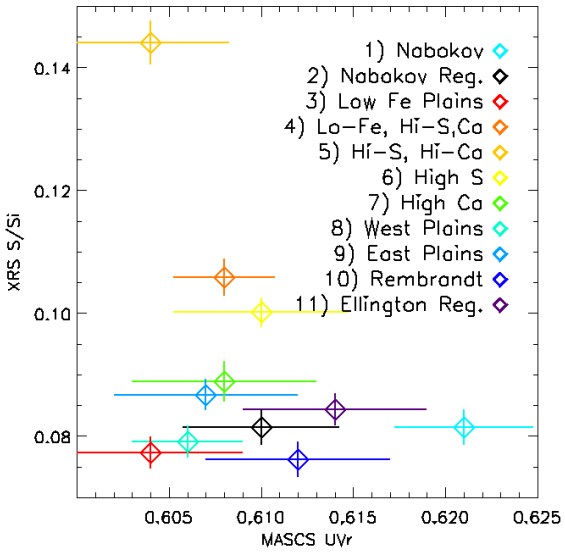

Figure 4. MASCS UVr versus XRS S/Si. There is a possible minor anticorrelation at higher S values.

References: [1] Solomon S. C. et al. (2001) *Planet. Space Sci. 49*, 1445–1465. [2] McClintock W. E. and Lankton, M. R. (2007) *Space Sci. Rev. 131*, 481–522. [3] Nittler L. R. et al. (2011) *Science 333*, 1847–1850. [4] Weider S. Z. et al. (2012) *JGR*, E00L05. [5] Weider S. Z. et al. (2013) *LPS 44*, this meeting. [6] Evans L. G. et al. (2012) *JGR*, E00L07. [7] Klima et al. (2013) *LPS 44,* this meeting. [8] Hawkins S. E., III, et al. (2007) *Space Sci. Rev. 131*, 247–338. [9] Izenberg N. R. et al. (2012) *AGU Fall Meeting*, abstract P31D-04. [10] Izenberg N. R. et al. (2013) *JGR*, in preparation. [11] Blewett D. T. et al. (2011) *Science 333*, 1856–1859. [12] Blewett D. T. et al. (2013) *JGR 118*, E004174. [13] Denevi B. W. et al. (2009) *Science 324*, 613–618.